

**SURFACE ENGINEERING OF TITANIUM BASED METAL FOR  
CELL INTERACTION**

**by**

**ROSHASNORLYZA BINTI HAZAN**

**Thesis submitted in fulfillment of the requirements**

**for the degree of**

**Doctor of Philosophy**

**UNIVERSITI SAINS MALAYSIA**

**September 2014**

## ACKNOWLEDGEMENT

Praise to ALLAH, His majesty for His uncountable blessings, and best prayers and peace onto His best messenger Mohammed, His pure descendant and his family and his noble companions.

This work was carried out at the School of Materials and Mineral Resources Engineering, Universiti Sains Malaysia in cooperation with the Advance Medical and Dental Institute (AMDI), Universiti Sains Malaysia during the years 2008-2014.

First, I would like to thank my supervisors Assoc. Prof. Ir. Dr. Srimala Sreekantan and Prof. Dr. Ishak Mat for valuable advice and criticism to this scientific research. Your help and guidance over the years which is immeasurable and without it I would not be where I am today. I thank you so much for the knowledge you have passed on and I will always be grateful for having the opportunity to study under you. I express my gratitude to Prof. Sumiko Watanabe for her generosity to supply PA6 cells for my research. I would also like to express my thanks to the dean of the School of Materials and Mineral Resources Engineering for their support ship to the student of higher education. I would like to thank all technicians in School of Materials and Mineral Resources Engineering for their assistance. I express my thanks to AMDI staff for helping me with the cell culture studies. Next, I would like to thank my family. My special thanks to my beloved husband, Sulaiman Mohammad for his support and encouragement throughout this hard time. During these years, the support of my friends has been extremely valuable especially their suggestion to improve my research. I would like to thanks everyone that helps me with this research either direct or indirectly. Without your help and co-operation, this research cannot be done.

Thank you.

## TABLE OF CONTENTS

	Page
<b>ACKNOWLEDGEMENT</b>	ii
<b>TABLE OF CONTENTS</b>	iii
<b>LIST OF TABLES</b>	ix
<b>LIST OF FIGURES</b>	xi
<b>LIST OF ABBREVIATIONS</b>	xx
<b>LIST OF SYMBOLS</b>	xxiii
<b>LIST OF PUBLICATIONS</b>	xxiv
<b>ABSTRAK</b>	xxviii
<b>ABSTRACT</b>	xxx
<b>CHAPTER 1 INTRODUCTION</b>	
1.1 Introduction	1
1.2 Problem statement	3
1.3 Objectives	6
1.4 Research outcomes	7
1.5 Structure of the thesis	7
<b>CHAPTER 2: LITERATURE REVIEW</b>	
2.1 Introduction	9
2.2 Ti as biomaterial	10

2.3	Physiological response to implanted materials	13
2.4	Biocompatibility of nanomaterials	13
	2.4.1 Titanium osseointegration	15
2.5	Cell-metal interaction	16
	2.5.1 Cell	18
	2.5.2 PA6 cels	21
2.6	Nano-scale surface engineering on Ti	21
	2.6.1 TiO <sub>2</sub> nanotube arrays	24
	2.6.2 TiO <sub>2</sub> nanotube arrays formation mechanism	26
	2.6.3 Factor affecting geometry of TiO <sub>2</sub> nanotube arrays	27
	2.6.4 Crystallization of TiO <sub>2</sub> nanotube arrays	31
2.7	Cellular response to TiO <sub>2</sub> nanotube arrays	32
	2.7.1 Cell behavior in different dimensionalities of TiO <sub>2</sub> nanotubes arrays	34
	2.7.2 Cell behavior in different crystal structures of TiO <sub>2</sub> nanotubes arrays	38
	2.7.3 Cell adhesion	40
	2.7.4 Mechanism of cell adhesion on TiO <sub>2</sub> nanotubes surface	41
	2.7.5 Differentiation of Mesenchymal Stem Cells (MSC)	42
	2.7.6 Protein adsorption on TiO <sub>2</sub> nanotube arrays	42
	2.7.7 Biomarker	45
2.8	Hydroxyapatite coating	45
2.9	Summary of chapter 2	47

## CHAPTER 3: METHODOLOGY

3.1	Introduction	49
3.2	Raw materials and apparatus	49
3.2.1.	Titanium (Ti) foil	49
3.2.2	Glycerol	49
3.2.3	Ammonium Fluoride (NH <sub>4</sub> F)	50
3.2.4	Ethanol	50
3.2.5	Sulphuric acid	51
3.2.6	Sodium hydroxide (NaOH)	51
3.2.7	Simulated Body Fluid (SBF)	51
3.2.8	Tetraspan 6 %	51
3.2.9	Complete $\alpha$ -MEM medium	52
3.2.10	Phosphate buffer saline (PBS)	52
3.2.11	PA6 cell lines (Bone Marrow Stromal Cells)	52
3.2.12	Typan Blue dye (0.4%)	53
3.2.13	Heamytometer	54
3.2.14	Trypsin	54
3.2.15	Dimethyl Sulfoxide (DMSO)	54
3.2.16	Glass Slide	55
3.2.17	Methanol	55
3.2.18	MTS assay	55
3.2.19	Glutaraldehyde	56
3.2.20	Alamar Blue Assay	56

3.2.21	Primary antibody	56
3.2.22	Propidium Iodide	56
3.2.23	Lysis Buffer	57
3.2.24	2-D Quant Kit	57
3.2.25	Sodium Dodecyl Sulphate Polyacrylamide Gel Electrophoresis (SDS-PAGE)	58
3.2.26	Immunophenotyping chemical	58
3.2.27	Western Blotting materials	58
3.2.28	Methylamine tungstate	59
3.2.29	Alkaline Phosphatase Activity (ALP) chemicals	59
3.2.30	Alizarin Red S (ARS) chemicals	60
3.3	Design of experiment	61
3.3.1	Part A: Effect of electrochemical parameters on TiO <sub>2</sub> nanotubes dimensionality	61
3.3.2	Part B: Effect of annealing to TiO <sub>2</sub> nanotubes crystal structure	63
3.3.3	Part C: Effect of TiO <sub>2</sub> nanotubes dimensionality and crystal structure on cell interaction	63
3.3.4	Part D: Effect of Hydroxyapatite (HA) formation on TiO <sub>2</sub> nanotubes to cell interaction	64
3.4	Experimental Procedure	64
3.4.1	Procedure of anodization experiment	64
3.4.2	Hydroxyapatite (HA) formation on TiO <sub>2</sub> nanotubes	67
3.4.3	Cell culture	68

3.5	Characterizations	72
3.5.1	Materials Characterization	74
3.5.2	Cell Interaction ( <i>in vitro</i> )	78

## **CHAPTER 4: RESULTS AND DISCUSSIONS**

4.1	Introduction	82
4.2	Part A: Effect of electrochemical parameters to TiO <sub>2</sub> nanotubes dimensionality	82
4.2.1	Effect of applied potential on the formation of TiO <sub>2</sub> nanotube arrays	83
4.2.2	Effect of anodization time	104
4.2.3	Effect of electrolyte pH	113
4.2.4	Summary of Part A	120
4.3	Part B: Effect of Annealing Temperature to TiO <sub>2</sub> Nanotubes Crystal Structure	121
4.3.1	Structural analyses of the annealed TiO <sub>2</sub> nanotube arrays	121
4.3.2	Surface morphology of the annealed TiO <sub>2</sub> nanotube arrays	129
4.3.3	Effect of annealing temperature of TiO <sub>2</sub> nanotubes to corrosion properties	132
4.3.4	Summary of Part B	135
4.4	Part C: Effect of TiO <sub>2</sub> nanotubes dimensionality and crystal structure to cell interaction	135
4.4.1	Effect of TiO <sub>2</sub> nanotubes diameter and length to cell interaction	135
4.4.2	Effect of TiO <sub>2</sub> nanotubes length to cell interaction	152

4.4.3 Effect of TiO <sub>2</sub> nanotubes crystal structure to cell interaction	156
4.4.4 In Vitro Materials Elution	166
4.4.5 Protein Adsorption	170
4.4.6 Biomarker	172
4.4.7 Immunophenotyping of PA6 cells	188
4.4.8 Summary of Part C	194
4.5 Part D: Effect of Hydroxyapatite (HA) formation on TiO <sub>2</sub> nanotubes to cell interaction	197
4.5.1 Hydroxyapatite (HA) formation on TiO <sub>2</sub> nanotubes by simulated body fluid soaking	197
4.5.2 Cell interaction study	205
4.5.3 Summary of Part D	207
<b>CHAPTER 5: CONCLUSION</b>	
5.1 Conclusion	208
5.2 Suggestion for future research	210
<b>REFERENCES</b>	212



<b>LIST OF TABLES</b>		<b>Page</b>
Table 2.1	List of biomaterials and its application.	<b>11</b>
Table 2.2	Mechanical properties of selected titanium biomaterials [Freese <i>et al.</i> , 2001].	<b>12</b>
Table 2.3	List of cell type selection to study cell-metal interaction and its information.	<b>20</b>
Table 2.4	List of surface engineering approaches to achieve geometrical structuring of TiO <sub>2</sub> surface.	<b>23</b>
Table 2.5	Summary of influence TiO <sub>2</sub> nanotubes diameter to cell-metal interaction.	<b>36</b>
Table 2.6	Summary of influence TiO <sub>2</sub> nanotubes crystal structure to cell-metal interaction.	<b>39</b>
Table 2.7	List of biomarker used to study cell-metal interaction.	<b>46</b>
Table 3.1	Chemical used to produce SBF solution	<b>52</b>
Table 3.2	Chemical used to produce complete medium	<b>53</b>
Table 3.3	List of primary antibody	<b>57</b>
Table 3.4	Lysis buffer chemical	<b>58</b>
Table 3.5	SDS-PAGE chemical	<b>59</b>
Table 3.6	Immunophenotyping chemicals	<b>59</b>
Table 3.7	Western Blotting materials	<b>60</b>
Table 3.8	ALP chemicals	<b>60</b>
Table 3.9	Alizarin Red S chemicals	<b>60</b>
Table 3.10	Constant parameter in anodization for potential variation	<b>62</b>
Table 3.11	Constant parameter to study effect of anodization time	<b>62</b>

Table 3.12	Constant parameter to study effect of electrolyte pH	<b>63</b>
Table 3.13	Ion concentration of human blood plasma and SBF	<b>67</b>
Table 3.14	Dimension and number of samples need for cell interaction study	<b>73</b>
Table 4.1	Geometric surface area ( <i>G</i> ) and aspect ratio ( <i>AR</i> ) for TiO <sub>2</sub> nanotubes produces at different voltages.	<b>91</b>
Table 4.2	Roughness for TiO <sub>2</sub> nanotubes anodized at different voltage	<b>94</b>
Table 4.3	Lattice parameter of TiO <sub>2</sub> nanotubes produced at different applied voltage and annealed at 400 °C for 2 hours.	<b>99</b>
Table 4.4	Electrochemical parameters of TiO <sub>2</sub> nanotube arrays produced at different applied voltage in Tetraspan electrolyte	<b>101</b>
Table 4.5	Growth rate of TiO <sub>2</sub> nanotubes formation	<b>110</b>
Table 4.6	The wavenumber (cm <sup>-1</sup> ) and intensity (arb. units) of the samples.	<b>128</b>
Table 4.7	Corrosion parameters tested in this research.	<b>134</b>
Table 4.8	Composition of the α-MEM solution used in this study	<b>167</b>
Table 4.9	Peak identity with JCPDS file for XRD spectra Figure 4.45	<b>170</b>
Table 4.10	Antibodies and isotypic control used for Immunophenotyping of PA6 cells	<b>189</b>
Table 4.11	The atomic % and Ca/P atomic ratios of TiO <sub>2</sub> nanotubes soaked in SBF for different duration and human bone.	<b>200</b>
Table 4.12	Electrochemical parameters of TiO <sub>2</sub> nanotube arrays with and without immersion in SBF solution.	<b>205</b>

<b>LIST OF FIGURES</b>		<b>Page</b>
Figure 2.1	Schematic comparison between natural tooth and implant tooth [Oshida, 2006]	<b>12</b>
Figure 2.2	Time line of the biological response to material surfaces [Jell <i>et al.</i> , 2009].	<b>14</b>
Figure 2.3	Model for cell alignment on surface substrate. (a) Focal adhesion and actin filament adhere to surface substrate. (b) Filopodia movements are isotropic on surface substrate. Adapted from Anselme <i>et al.</i> , 2010.	<b>17</b>
Figure 2.4	Scanning electron micrograph showing a multilayer of rat bone marrow cells and extracellular matrix covering the substrate surface [Knabe <i>et al.</i> , 2002]. Bar = 20mm.	<b>18</b>
Figure 2.5	Scanning Electron microscope (SEM) images of top and cross section of TiO <sub>2</sub> nanotubular structure grown in a mixture of glycerol and water (60:40 vol%) + 0.27 M NH <sub>4</sub> F electrolyte at 30 V, after annealing to anatase ((a), (b)). Adapted from Paramasivam <i>et al.</i> , 2009.	<b>25</b>
Figure 2.6	TiO <sub>2</sub> nanotubes formation process stages [Macak <i>et al.</i> , 2007].	<b>27</b>
Figure 2.7	The effect of voltage on the surface of the anodization titanium (0.24 mol l <sup>-1</sup> H <sub>2</sub> SO <sub>4</sub> + 0.5 wt% NH <sub>4</sub> F, 60 min) (a)20V;(b)30V [Tian <i>et al.</i> , 2007].	<b>28</b>
Figure 2.8	Field emission scanning electron microscope (FESEM) cross-section of TiO <sub>2</sub> nanotube array anodic growth at 30 V for (a) 14 h, (b) 30 h, and (c) 40 h. High-magnification images are shown in the insets of the pictures. The arrows indicate the length of the nanotubes. (d) Nanotube length as a function of the anodization reaction time (Yang <i>et al.</i> , 2008b).	<b>29</b>
Figure 2.9	SEM top-view and cross-sectional view of TiO <sub>2</sub> nanotubes for various pH values of the electrolyte. The composition of all of the electrolytes is identical. (a) pH 1.5, (b) pH 3, (c) pH 4.2, and (d) pH 5 (Kang <i>et al.</i> , 2008).	<b>30</b>
Figure 2.10	(a) X-ray diffraction (XRD) profiles and (b) Raman spectra of TiO <sub>2</sub> nanotube arrays after heating at different temperatures for 2 h in air (Fang <i>et al.</i> , 2008).	<b>32</b>

Figure 2.11	(a) SEM micrographs of bovine aortic endothelial cells on Ti and (b) on TiO <sub>2</sub> surfaces after 2h of culture. A much more pronounced protrusion of filopodia with significantly longer configuration and a high degree of contact is seen on the TiO <sub>2</sub> nanotube surface (Brammer <i>et al.</i> , 2008).	<b>34</b>
Figure 2.12	Schematic illustration of the mechanism by which nanomaterials may be superior to conventional materials for bone regeneration [Zhang and Webster, 2009].	<b>34</b>
Figure 2.13	MTT test on the influence of livability of C6 glioma cell on TiO <sub>2</sub> nanotube array (*p< 0.05) (Yang <i>et al.</i> , 2013).	<b>35</b>
Figure 2.14	MTT assay data showing the optical density (OD) of reaction product of the MTT working solution with osteoblast cells cultured using flat Ti, as-formed and annealed TiO <sub>2</sub> nanotubes after 2, 3 and 4 days of incubation. Significant difference p<0.05 compared with TiO <sub>2</sub> nanotubes. Significant difference p <0.05 compared with annealed nanotubes. Significant difference p<0.05 compared with mixture anatase-rutile of TiO <sub>2</sub> nanotubes [Bai <i>et al.</i> , 2010].	<b>38</b>
Figure 2.15	Differentiation of HSC from bone marrow cells (Adapted from <a href="http://hepatitiscnewdrug.blogspot.com">hepatitiscnewdrug.blogspot.com</a> ).	<b>43</b>
Figure 2.16	Differentiation of MSC into specific cell functionality. (Adapted from <a href="http://pdwrites.com">pdwrites.com</a> )	<b>43</b>
Figure 2.17	Schematic representation of the interaction of cells with proteins adsorbed on a substrate such as an implant (Ejiofor and Webster, 2004).	<b>44</b>
Figure 2.18	SEM of coating surface after immersion in SBF 7 days. Inserts show EDAX of the SBF-treated coating surfaces [Tsuchiya <i>et al.</i> , 2006].	<b>48</b>
Figure 3.1	Heamytometer	<b>54</b>
Figure 3.2	Flow chart for anodization procedure	<b>64</b>
Figure 3.3	Anodization setup	<b>66</b>
Figure 3.4	Grooves of the counting area on Heamocytometer	<b>69</b>
Figure 3.5	Grid on heamocytometer	<b>70</b>

Figure 3.6	Cell interaction characterization	<b>73</b>
Figure 3.7	Schematic of TiO <sub>2</sub> nanotubes dimensionality. $\varnothing_o$ = outer diameter; $\varnothing_i$ = inner diameter; $w$ = wall thickness; and $L$ = nanotubes length.	<b>75</b>
Figure 4.1	Current density of anodized Ti foil at different voltage; (a) 5 V, (b) 10 V, (c) 20 V, (d) 30 V, and (e) 60 V	<b>84</b>
Figure 4.2	Magnification of graph in Figure 4.2; current density of anodized Ti foil at (a) 30 V and (b) 60 V.	<b>85</b>
Figure 4.3	SEM micrograph of anodized Ti foil at different voltage; (a) as received Ti foil, (b) 1 V, (c) 5 V, (d) 10 V, (e) 20 V, (f) 30 V, (g) 40 V, (h) 50 V and (i) 60 V.	<b>87</b>
Figure 4.4	(a) SEM micrograph and (b) EDX spectra of Ti foil anodized at 1 V.	<b>89</b>
Figure 4.5	Dimension of TiO <sub>2</sub> nanotubes produce at different voltage.	<b>90</b>
Figure 4.6	TEM micrograph of TiO <sub>2</sub> nanotubes produced at 40 V.	<b>92</b>
Figure 4.7	AFM images of Ti surface after anodization at (a) 10 V, (c) 20 V, (e) 30 V, (g) 40 V, (i) 50 V and (k) 60 V. The graph on the right is linear profile for the image respectively. [* - indicating tube wall disintegrates]	<b>93</b>
Figure 4.8	XRD of as-anodized samples produced at different voltage; (a) Ti, (b) 1 V, (c) 5 V, (d) 10 V, (e) 20 V, (f) 30 V, (g) 40 V, (h) 50 V and (i) 60 V (■: Ti).	<b>97</b>
Figure 4.9	XRD of TiO <sub>2</sub> nanotubes annealed at 400 °C; (a) 1 V, (b) 5 V, (c) 10 V, (d) 20 V, (e) 30 V, (f) 40 V, (g) 50 V and (h) 60 V (■: Ti and ▲: Anatase). The insert shows the magnified pattern of (101) plane peak.	<b>98</b>
Figure 4.10	Potentiodynamic corrosion curves of TiO <sub>2</sub> nanotube arrays produced at different applied voltage; (a) 10 V, (b) 20 V, (c) 30 V, (d) 40 V and (e) Ti foil in Tetraspan electrolyte	<b>100</b>
Figure 4.11	Current density vs. time during anodization of Ti in glycerol + 0.5 wt% NH <sub>4</sub> F solutions at 30 V.	<b>105</b>

Figure 4.12	Evolution of nano-tubular oxide layer during anodization of Ti in glycerol + 0.5 wt % NH <sub>4</sub> F solutions at 30 V for (a) 10 s, (b) 1 min, (c) 2 min, (d) 5 min, (e) 10 min, (f) 20 min, (g) 30 min, (h) 1 h, (i) 2 h, (j) 3 h and (k) 6 h.	<b>105</b>
Figure 4.13	TiO <sub>2</sub> nanotube layers (a) anodized for 3 h and (b) peel off after 6 h of anodization in glycerol + 0.5 wt% NH <sub>4</sub> F.	<b>109</b>
Figure 4.14	Correlation of TiO <sub>2</sub> nanotubes length and inner diameter with regard of anodization time. The triangles indicate the growth rate of TiO <sub>2</sub> nanotubes at 3 different stages.	<b>110</b>
Figure 4.15	XRD patterns of as-anodized TiO <sub>2</sub> nanotubes in glycerol electrolytes for (a) 5 min, (b) 1 h and (c) 3 h. (A: Anatase; T: Titanium)	<b>112</b>
Figure 4.16	Raman spectra of TiO <sub>2</sub> nanotube arrays anodized for (a) 1 h and (b) 3h in glycerol and NH <sub>4</sub> F electrolyte.	<b>113</b>
Figure 4.17	<i>I-t</i> curve of Ti anodized in electrolyte with different pHs: (a) pH 1, (b) pH 6 and (c) pH 8.	<b>114</b>
Figure 4.18	Microstructural topography at different electrolyte pH (a) pH 1, (b) pH 2, (c) pH 3, (d) pH 4, (e) pH 5, (f) pH 6, (g) pH 7, (h) pH 8 and (i) pH 9	<b>117</b>
Figure 4.19	Correlation of TiO <sub>2</sub> nanotubes length with regards of pH value.	<b>119</b>
Figure 4.20	XRD patterns of (a) as-anodized and annealed TiO <sub>2</sub> nanotube arrays at (b) 200 °C, (c) 300 °C, (d) 400 °C, (e) 500 °C, (f) 600 °C, (g) 700 °C, (h) 800 °C and (i) 900 °C. A, R and T represent anatase, rutile and titanium, phase respectively.	<b>122</b>
Figure 4.21	Magnified patterns of anatase (101) crystallographic plane.	<b>123</b>
Figure 4.22	Magnified patterns of anatase (004) crystallographic plane at 38.54°.	<b>124</b>
Figure 4.23	Raman spectra of TiO <sub>2</sub> nanotube arrays for (a) as anodized and after annealing at different temperature: (b) 200 °C, (c) 300 °C, (d) 400 °C, (e) 500 °C, (f) 600 °C and (g) 700 °C for 2 hours in air.	<b>126</b>
Figure 4.24	FESEM images of TiO <sub>2</sub> nanotube arrays anodized at 20 V after annealing at (a) 200 °C, (b) 300 °C, (c) 400 °C, (d) 500 °C, (e) 600 °C, (f) 700 °C, (g) 800 °C and (h) 900 °C.	<b>130</b>

Figure 4.25	Potentiodynamic polarization plot recorded for TiO <sub>2</sub> nanotubes; (a) as-anodized, annealing at (b) 400 °C, (c) 600 °C and (d) 700 °C.	<b>134</b>
Figure 4.26	Fluorescence images of cells attached after 3 days of incubation; (a) glass, (b) Ti, (c) 10 V, (d) 20 V, (e) 30 V and (f) 40 V. The PA6 cells were stained with CD 34 (green) and PI (red).	<b>136</b>
Figure 4.27	Adherent PA6 cell numbers measured by counting cells stained with PI under a fluorescence microscope after 1 and 3 days of incubation. * indicates statistical significance $p < 0.01$ compared to other surfaces.	<b>138</b>
Figure 4.28	FESEM pictures showing the morphology of PA6 cells after 1 and 14 days of culture on samples. Pictures with low magnification of 500x (the first and last column) show the overall view. Pictures of higher magnification display the detail of cell interaction with the micro/nanotopographies. Red arrow indicates abundant filopodia extension on samples and anchor to the nanotubes hole. Dotted line show cell outline (yellow indicate rounded cells and green indicate polygonal shape cells) on samples.	<b>139</b>
Figure 4.29	Cell viability of PA6 cells on different TiO <sub>2</sub> nanotubes diameter. *** $p < 0.001$ : considered very significant and ** $p < 0.01$ : considered significantly different after 1 and 7 days of culture.	<b>144</b>
Figure 4.30	Temporal changes in Alamar Blue reduction on different surfaces cultured with PA6 cells.	<b>145</b>
Figure 4.31	(a) ALP standard curves. (b) Quantitative ALP analyses at day 3 and 7. Values are represented as the mean $\pm$ SEM, N = 3, * $p < 0.05$ and *** $p < 0.001$ compared to glass substrate at the same time period.	<b>148</b>
Figure 4.32	(a) ARS standard curves. (b) Calcium deposition by PA6 cells on the samples of interest to the present study.	<b>149</b>
Figure 4.33	Schematic diagram of calcium and phosphate deposition on the TiO <sub>2</sub> nanotubes sample.	<b>150</b>
Figure 4.34	FESEM views of PA6 cells after 3 days of culture on different TiO <sub>2</sub> nanotubes length: (a) 0.22 $\mu\text{m}$ sample and (b) 2.21 $\mu\text{m}$ sample. The arrows indicate cell spreading direction.	<b>153</b>
Figure 4.35	Cell viability of PA6 cells on different TiO <sub>2</sub> nanotubes length. * $p < 0.001$ : considered very significant in different after 1 and 3 days of culture.	<b>154</b>

Figure 4.36	Upper panel shows the fluorescence images of cells attached after 3 days of incubation; (a) short and (b) long TiO <sub>2</sub> nanotubes. (c) Adherent PA6 cell numbers measured by counting cells stained with PI under a fluorescence microscope after 1 and 3 days of incubation. * indicates statistical significance $p < 0.01$ compared to other surfaces.	<b>155</b>
Figure 4.37	Quantitative ALP analyses at day 7. Values are represented as the mean $\pm$ SEM, N = 3, * $p < 0.05$ and *** $p < 0.001$ compared to glass substrate at the same time period.	<b>157</b>
Figure 4.38	FESEM micrograph of (a-b) glass and TiO <sub>2</sub> nanotubes with different crystal structure (c-d) amorphous, (e-f) anatase, (g-h) mixed anatase-rutile and (i-j) rutile phase after 1 and 3 days PA6 cells incubation.	<b>158</b>
Figure 4.39	Higher magnification of FESEM micrograph of (a-b) glass and TiO <sub>2</sub> nanotubes with different crystal structure (c-f) amorphous, (g-j) anatase, (k-n) mixed anatase-rutile and (o-r) rutile phase after 1 and 3 days PA6 cells incubation. The red arrows indicate filopodia.	<b>160</b>
Figure 4.40	PA6 cells viability on different phases of TiO <sub>2</sub> nanotube surfaces determined by the MTS assay.	<b>162</b>
Figure 4.41	Temporal changes in Alamar Blue reduction on different phases of TiO <sub>2</sub> nanotubes cultured with PA6 cells.	<b>163</b>
Figure 4.42	Fluorescence images of PA6 cells attached after 3 days of incubation stained with CD34 and PI; (a) amorphous, (b) anatase, (c) anatase-rutile mixture and (d) rutile phase of TiO <sub>2</sub> nanotubes.	<b>164</b>
Figure 4.43	Adherent PA6 cell numbers measured by counting cells stained with PI under a fluorescence microscope after 3 days of incubation. * indicates statistical significance $p < 0.01$ compared to other surfaces. Upper panel shows the fluorescence images of cells attached after 3 days of incubation; (a) amorphous, (b) anatase, (c) anatase-rutile mixture and (d) rutile phase of TiO <sub>2</sub> nanotubes.	<b>165</b>
Figure 4.44	ALP activity of PA6 cells cultured on different phases of TiO <sub>2</sub> nanotubes after 7 days of incubation (Value are mean $\pm$ SEM, $n=3$ ). * $p < 0.05$ compared with glass and *** $p < 0.001$ compared with other sample.	<b>166</b>
Figure 4.45	XRD spectra of two different solution after in vitro testing, (a) $\alpha$ -MEM solution only and (b) $\alpha$ -MEM solution with glass; (c) $\alpha$ -MEM solution with TiO <sub>2</sub> nanotube arrays and (d) XRD spectra for	<b>169</b>



TiO<sub>2</sub> nanotube arrays. ( $\alpha$ : $\alpha$ -Ca<sub>2</sub>P<sub>2</sub>O<sub>7</sub>, A: Anatase, B:Brushite, Ca:Calcium, Ca<sub>10</sub>:Ca<sub>10</sub> Hydroxyapite, HAp:Hydroxapatite, M:Monetite, Mg:Magnesium and Ti: Ti)

Figure 4.46	Protein concentrations of PA6 cells cultured on the substrates (TiO <sub>2</sub> nanotubes, unmodified Ti and control surface) after 3 days incubation. Values are represented as the mean $\pm$ SEM, N = 6. * <i>p</i> < 0.05 compared to each samples.	<b>171</b>
Figure 4.47	1-D SDS-Page of PA6 cells cultured on TiO <sub>2</sub> nanotubes, Ti and glass after 3 days incubation.	<b>173</b>
Figure 4.48	Densitometry of PA6 cells protein after cultured on TiO <sub>2</sub> nanotubes, Ti and glass for 3 days.	<b>173</b>
Figure 4.49	PA6 cells without antibody (left) and stained with IgM (right) under a fluorescence microscope after 3 days of incubation; (a-b) glass, (c-d) Ti and (d-e) TiO <sub>2</sub> nanotubes, $\times$ 100.	<b>175</b>
Figure 4.50	PA6 cells stained with cytokeratin under a fluorescence microscope after 3 days of incubation; (a) glass, (b) Ti and (c) TiO <sub>2</sub> nanotubes, $\times$ 100.	<b>176</b>
Figure 4.51	Western blot analysis of cytokeratin marker expressed by PA6 cells cultured on glass, Ti and TiO <sub>2</sub> nanotubes.	<b>177</b>
Figure 4.52	The Western Blot band intensity analyses by densitometer of the cytokeratin marker expressed by PA6 cells at 52 kDa for glass, Ti and TiO <sub>2</sub> nanotubes using Versa Doc software.	<b>178</b>
Figure 4.53	PA6 cells stained with BrDU under a fluorescence microscope after 3 days of incubation; (a) glass, (b) Ti and (c) TiO <sub>2</sub> nanotubes, $\times$ 100.	<b>180</b>
Figure 4.54	Western Blot analysis of BrDU marker expressed by PA6 cells cultured on glass, Ti and TiO <sub>2</sub> nanotubes.	<b>180</b>
Figure 4.55	The Western Blot band intensity analyses by densitometer of the BrDU marker expressed by PA6 cells at 30 kDa for glass, Ti and TiO <sub>2</sub> nanotubes using versa Doc software.	<b>181</b>
Figure 4.56	Western Blot analysis of CD13 marker expressed by PA6 cells cultured on glass, Ti and TiO <sub>2</sub> nanotubes.	<b>182</b>
Figure 4.57	PA6 cells stained with CD34 under a fluorescence microscope after 3 days of incubation; (a) glass, (b) Ti and (c) TiO <sub>2</sub> nanotubes, $\times$	<b>183</b>

100.

Figure 4.58	Western Blot analysis of CD34 marker expressed by PA6 cells cultured on glass, Ti and TiO <sub>2</sub> nanotubes.	<b>183</b>
Figure 4.59	The Western Blot band intensity analyses by densitometer of the CD34 marker expressed by PA6 cells at 34 kDa for glass, Ti and TiO <sub>2</sub> nanotubes using versa Doc software.	<b>184</b>
Figure 4.60	PA6 cells stained with CD117 under a fluorescence microscope after 3 days of incubation; (a) glass, (b) Ti and (c) TiO <sub>2</sub> nanotubes, × 100.	<b>185</b>
Figure 4.61	PA6 cells stained with IBMR3 under a fluorescence microscope after 3 days of incubation; (a) glass, (b) Ti and (c) TiO <sub>2</sub> nanotubes, × 100.	<b>186</b>
Figure 4.62	Western Blot analysis of IBMR3 marker expressed by PA6 cells cultured on glass, Ti and TiO <sub>2</sub> nanotubes.	<b>187</b>
Figure 4.63	The Western Blot band intensity analyses by densitometer of the IBMR3 marker expressed by PA6 cells at 38, 190, 273 and 356 kDa for glass, Ti and TiO <sub>2</sub> nanotubes using versa Doc software.	<b>187</b>
Figure 4.64	PA6 cells stained with PI under a fluorescence microscope after 3 days of incubation; (a) glass, (b) Ti and (c) TiO <sub>2</sub> nanotubes, × 100.	<b>188</b>
Figure 4.65	Phenotype analyses of PA6 cells. PA6 cells were analyzed by fluorescence-activated sorting (FACS) with antibody against CD 13 and isotype control IgG <sub>1</sub> as indicated. <b>A</b> PA6 cells cultured on plastic control. <b>B</b> PA6 cells cultured on TiO <sub>2</sub> nanotubes.	<b>190</b>
Figure 4.66	Phenotype analyses of PA6 cells. PA6 cells were analyzed by fluorescence-activated sorting (FACS) with antibody against CD51. <b>A</b> PA6 cells cultured on plastic control. <b>B</b> PA6 cells cultured on TiO <sub>2</sub> nanotubes.	<b>191</b>
Figure 4.67	Phenotype analyses of PA6 cells. PA6 cells were analyzed by fluorescence-activated sorting (FACS) with antibody against CD49e and isotype control IgG <sub>2a</sub> as indicated. <b>A</b> PA6 cells cultured on plastic control. <b>B</b> PA6 cells cultured on TiO <sub>2</sub> nanotubes.	<b>192</b>
Figure 4.68	Phenotype analyses of PA6 cells. PA6 cells were analyzed by fluorescence-activated sorting (FACS) with antibody against CD73. <b>A</b> PA6 cells cultured on plastic control. <b>B</b> PA6 cells cultured on TiO <sub>2</sub> nanotubes.	<b>193</b>

Figure 4.69	Phenotype analyses of PA6 cells. PA6 cells were analyzed by fluorescence-activated sorting (FACS) with antibody against CD117 and isotype control IgG <sub>2b</sub> as indicated. <b>A</b> PA6 cells cultured on plastic control. <b>B</b> PA6 cells cultured on TiO <sub>2</sub> nanotubes.	<b>195</b>
Figure 4.70	FESEM micrograph of TiO <sub>2</sub> nanotube arrays soaked in SBF: (a) 0, (b) 3, (c) 7 and (d) 14 days.	<b>198</b>
Figure 4.71	EDX spectra of TiO <sub>2</sub> nanotubes soaked in SBF for; (a) 3, (b) 7 and (c) 14 days.	<b>199</b>
Figure 4.72	Weight gains of TiO <sub>2</sub> nanotubes after immersion in SBF.	<b>200</b>
Figure 4.73	EDX spectra of TiO <sub>2</sub> nanotubes soaked in SBF for 21 days.	<b>201</b>
Figure 4.74	XRD patterns of TiO <sub>2</sub> nanotubes after soaking in SBF for 14 days (T: Ti, A: Anatase and H: HA).	<b>202</b>
Figure 4.75	FTIR spectra for TiO <sub>2</sub> nanotubes after immersion into SBF for 14 days.	<b>203</b>
Figure 4.76	Potentiodynamic corrosion curves of TiO <sub>2</sub> nanotube arrays (a) without and (b) with immersion in SBF solution.	<b>205</b>
Figure 4.77	FESEM pictures showing the morphology of PA6 cells after 3 days of culture on (a-b) TiO <sub>2</sub> nanotubes and (c-d) TiO <sub>2</sub> nanotubes immerse in SBF for 7 days. Pictures with low magnification of 200x (the first) show the overall view. Pictures of higher magnification display the detail of cell interaction with the micro/nanotopographies.	<b>206</b>
Figure 4.78	Cell viability of PA6 cells on control, TiO <sub>2</sub> nanotubes and TiO <sub>2</sub> nanotubes immerse in SBF. ** $p < 0.001$ : considered very significant and * $p < 0.01$ : considered significantly different after 1, 3 and 7 days of culture.	<b>207</b>

## LIST OF ABBREVIATIONS

1-D	One dimensional
3-D	Three dimensional
$\alpha$ -MEM	Minimum Essential Medium
$\beta$ ME	B-mercaptoethanol
A	Anatase
AB	Alamar Blue
AFM	Atomic force microscope
Al	Aluminium
ALP	Alkaline phosphatase
AMDI	Advanced Medical and Dental Institute
ANOVA	One-way analysis of variance
APS	Ammonium persulfate
AR	Aspect ratio
ARS	Alizarin Red-S
ATP	adenosine triphosphate
BMSC	bone marrow stromal cells
BrdU	bromodeoxyuridine
BSA	bovine serum albumin
Ca	Calcium
CaCl	Calcium Chloride
CD	Cluster of differentiation
CK	Cytokeratin
Cl	Chlorine
CFU	Colony-forming unit
CO <sub>2</sub>	Carbon dioxide
CSF	Cerebral spinal fluid
DAB	3,3'-diaminobenzidine
dc	Direct current
DMSO	Dimethyl sulfoxide
DTT	Dithiothreitol
EC	endothelial cells

ECM	Extra cellular matrix
EDX	Energy dispersive X-ray spectroscopy
F	Fluoride
Fe	Ferum
Fe <sub>3</sub> O <sub>4</sub>	Ferum Oxide
FESEM	Field emission scanning electron microscope
FTIR	Fourier transform infrared spectroscopy
FWHM	Full width half maximum
H	Hydrogen
H <sub>2</sub> O <sub>2</sub>	Hydrogen peroxide
H <sub>2</sub> SO <sub>4</sub>	Sulphuric acid
HA	Hydroxyapatite
HCl	Hydrochloride acid
HF	Hydrofluoric acid
HGF	Human gingival fibroblasts
hMSC	human bone marrow stem cells
HNEpC	Human nasal epithelial cells
HRB	Hardness, Rockwell B Scale
HRC	Hardness, Rockwell C Scale
HSC	Hematopoietic stem cells
IL	Human interleukin receptor
ISCT	International Society of Cell Therapy
JCPDS	Joint Committee on Powder Diffraction Standards
K	Potassium
KCl	Potassium Chloride
Mg	Magnesium
Mo	Molibdenum
MSC	Mesencymal stem cells
MTS	(3 - (4, 5 – dimethylthiazol – 2 - yl)-5-(3-carboxymethoxyphenyl)-2-(4-sulfophenyl)-2H-tetrazolium)
Na	Sodium
Na <sub>2</sub> SO <sub>4</sub>	Sodium sulphate
NaCl	Sodium Chloride

NaHCO <sub>3</sub>	Sodium bicarbonate
NB	Nanobacteria
Nb	Niobium
NH <sub>4</sub> F	Ammonium fluoride
NPC	Neural progenitor cells
O	Oxygen
O <sub>2</sub>	Oxide
OCPI	Osteoblastic precursor cell line
P	Phosphorus
PAEKs	Polyaryletherketones
PI	Propidium iodide
PMS	phenazine methosulfate
R	Rutile
ROS	Radical Oxidative Stress
SBF	Simulated body fluid
SDS-PAGE	Sodium Dodecyl Sulphate Polyacrylamide Gel Electrophoresis
SEM	Scanning electron microscope
Ta	Tantalum
TEM	Transmission electron microscope
Ti	Titanium
TiO <sub>2</sub>	Titanium dioxide
TNF	Tumor necrosis factor
USM	Universiti Sains Malaysia
V	Vanadium
VSMC	vascular smooth muscle cells
WHO	World Health Organization
XRD	X-ray diffraction
Zr	Zirconium

## LIST OF SYMBOLS

cm	centimeter
$E_{\text{corr}}$	Potential where current density increases with increasing potential
f	Mass fraction percent
g	gram
G	Geometric surface area factor
h	hour
$I_{\text{corr}}$	Corrosion current density
$I_{\text{pass}}$	Passive current density
k	constant
kDa	kilodalton
keV	Kiloelectron volt
L	Nanotube length
M	Molar
mA	Miliampere
MPa	Mega Pascal
min	Minute
nm	Nanometer
$R_a$	Average roughness
V	Voltage
w	Wall thickness
wt%	Weight percent
$\varnothing_i$	Inner diameter
$\varnothing_o$	Outer diameter
$\lambda$	Wavelength
$\beta$	FWHM in radian
$\theta$	Angle position of plane peak in radian
$\mu\text{m}$	Micrometer
$^{\circ}\text{C}$	Degree Celsius

## LIST OF PUBLICATIONS

### Patents:

1. Sreekantan, S., Arifin, Z. A., Lockman, Z., Lai, C. W., **Hazan, R.** and Saharudin, K. A. (2012). An apparatus and method for rapid rate of titanium oxide (TiO<sub>2</sub>) nanotube arrays formation, International application published under the Patent Cooperation Treaty (PCT), *International Patent Publication*. Number WO/2012/026799. Priority number: PI201004009.
2. Sreekantan, S., Arifin, Z. A., Lockman, Z., Lai, C. W., **Hazan, R.** and Saharudin, K. A. (2012). An apparatus and method for rapid rate of titanium oxide (TiO<sub>2</sub>) nanotube arrays formation, International application published under the Patent Cooperation Treaty (PCT), *Intellectual Property Corporation of Malaysia*, Filing number: PI201004009.

### Published papers in refereed journals:

1. Sreekantan, S., **Hazan, R.**, and Lockman, Z. (2009). Photoactivity of Anatase-Rutile TiO<sub>2</sub> Nanotubes at Various Annealing Temperature, *Thin Solid Film* 518; p. 16-21.
2. Sreekantan, S., Lockman, Z., **Hazan, R.**, Tasbihi, M., Lee, K. T., Mohamed, A. R. (2009). Influence of Electrolyte pH on TiO<sub>2</sub> Nanotube Formation by Ti Anodization, *Journal of Alloys and Compounds* 485; p. 478-483.
3. **Hazan, R.**, Sreekantan, S., Abdul Khalil, A., Nordin, I. M. S. and Mat, I. (2009). Surface Engineering of Titania for Excellent Fibroblast 3T3 Cell-Metal Interaction, *Journal of Physical Science*, 20; p. 35-47.
4. Sreekantan, S., **Hazan, R.**, and Lockman, Z. (2009). Synthesis, characterization and photocatalytic activity of TiO<sub>2</sub> nanotubes produced at various voltage, *Solid State Science and Technology* 17; p.132 – 139.
5. Sreekantan, S., **Hazan, R.**, Saharudin, K. A. and Mat, I. (2009). TiO<sub>2</sub> nanotubes arrays: formation and cell interactions studies, *MicroSoM* p. 7-9.
6. Sreekantan, S., **Hazan, R.**, Lockman, Z. and Mat, I. (2010). A study on preparation and characterization of carbon doped TiO<sub>2</sub> nanotubes, *Journal of Fundamental Sciences* 6; p.1- 8.
7. Sreekantan, S., **Hazan, R.**, Saharudin, K. A., Lai, C. W. and Mat, I., (2011). Formation of high aspect ratio TiO<sub>2</sub> nanotube arrays by anodization of Ti foil in organic solution, *Sains Malaysiana* 40; p. 227-230.



8. **Hazan, R.**, Sreekantan, S., Abdul Khalil, A., Nordin, I. M. S., Mat, I., (2011), TiO<sub>2</sub> foam: Characterization and Cell Adhesion, *Advanced Materials Research* 264-265; p. 1506-1513.
9. Saharudin, K. A., Sreekantan, S., Abd Aziz, S. N. Q. A., **Hazan, R.**, Lai, C. W., Mydin, R. B. S. M. N. and Mat, I. (2012), Surface Modification and Bioactivity of Anodic Ti6Al4V Alloy, *Journal of Nanoscience and Nanotechnology* 12; p. 1-10.
10. Sreekantan, S., **Hazan, R.**, Lockman, Z. and Mat. I., (2012), TiO<sub>2</sub> Nanotubes as a Novel Photocatalyzer and Excellent Implant Materials for Future Use. In Othman, R. and Sreekantan, S., ed. *Materials Engineering in Health Sciences*. Malaysia: Universiti Sains Malaysia Press, p. 9-17.
11. **Hazan, R.**, Sreekantan, S., Abdul Khalil, A., Nordin, I., M. S. and Mat, I., (2012), Fibroblast Cell Behavior on Porous Titania Thin Film. In Radzali Othman and Srimala Sreekantan, ed. *Materials Engineering in Health Sciences*. Malaysia: Universiti Sains Malaysia Press, p. 50-57.

#### **Published papers in national journal:**

1. Sreekantan, S., Ahmad, Z. A., **Hazan, R.** and Saharudin, K. A. (2009). TiO<sub>2</sub> Nanotubes Arrays (TiNA) –An Ultimate Smoke Purifier. *Enjinier* 11; p. 15.

#### **Conference proceedings:**

1. Sreekantan, S., **Hazan, R.** and Lockman, Z. (2008). Influence of Mixing Ratio of Anatase/Rutile TiO<sub>2</sub> on the Degradation of Methelyne Orange. *6<sup>th</sup> International Materials Technology Conference & Exhibition (IMTCE 2008)*, 24-27<sup>th</sup> Aug 2008, Park Royal Hotel, Kuala Lumpur, Malaysia.
2. Sreekantan, S., **Hazan, R.** and Lockman, Z. (2008). Synthesis, Characterization and Photocatalytic Activity of TiO<sub>2</sub> Nanotube Produced at Various Voltage. *Regional Conference on Solid State Science and Technology (RCSSST) 2008*, 30<sup>th</sup> Nov-2<sup>nd</sup> Dec 2008, Tiara Beach Resort, Port Dickson, Negeri Sembilan, Malaysia.
3. **Hazan, R.**, Sreekantan, S., Abdul Khalil, A., Nordin, I. M. S. and Mat, I. (2008). Synthesis of TiO<sub>2</sub> Nanotubes and Cell Interaction of Bone Marrow. *17<sup>th</sup> Electron Microscopy Society Malaysia (EMSM)*, 18-20<sup>th</sup> Dec 2008, Holiday Glenmarie, Shah Alam, Selangor, Malaysia.
4. **Hazan, R.**, Sreekantan, S., Abdul Khalil, A., Nordin, I. M. S. and Mat, I. (2009). Fibroblast Cell Behavior on Porous Titania Thin Film. *The 1<sup>st</sup> AUN/SEED-Net Regional Conference on Materials 2009 (RCM 2009)*, 16-17<sup>th</sup> Feb 2009, Equatorial Hotel, Penang, Malaysia.

5. Sreekantan, S., **Hazan, R.** and Lockman, Z. (2009). Titania Nanotubes: As an Novel Photocatalyzer and Excellent Implant Materials for Future. *The 1<sup>st</sup> AUN/SEED-Net Regional Conference on Materials 2009 (RCM 2009)*, 16-17<sup>th</sup> Feb 2009, Equatorial Hotel, Penang, Malaysia.
6. **Hazan, R.**, Sreekantan, S., Abdul Khalil, A., Nordin, I. M. S. and Mat, I. (2009). TiO<sub>2</sub> Foam: Characterization and Cell Adhesion. *The International Conference on Advanced Materials and Processing Technologies 2009 (AMPT 2009)*, 26-29<sup>th</sup> Oct 2009, Legend Hotel, Kuala Lumpur, Malaysia.
7. Sreekantan, S., **Hazan, R.**, Saharudin, K. A., Lai, C. W. and Mat, I. (2009). Formation of High Aspect Ratio TiO<sub>2</sub> Nanotube Arrays by Anodization of Ti Foil in Organic Solution. *Nanotech Malaysia 2009*, 26-29<sup>th</sup> Oct 2009, Kuala Lumpur Convention Centre, Kuala Lumpur, Malaysia.
8. **Hazan, R.**, Sreekantan, S., Abdul Khalil, A., Nordin, I. M. S. and Mat, I. (2009). TiO<sub>2</sub> Nanotubes on Ti Alloys – An Excellent Implant Metals. *2<sup>nd</sup> Translational Research Network (TRN) Workshop*, 30<sup>th</sup> Oct 2009, Seri Pacific Hotel, Kuala Lumpur, Malaysia.
9. **Hazan, R.**, Ah Barudin, N. H., Sreekantan, S. and Mat, I. (2009). Tailoring the Photocatalytic Activity of Titania Nanotubes Arrays: Effect of Time and Fluoride Contain. *Nanomaterials Synthesis & Characterization Conference (nMSC 2009)*, 3<sup>rd</sup>-4<sup>th</sup> Nov 2009, Palace of The Golden Horses, Selangor, Malaysia.
10. Sreekantan, S., **Hazan, R.**, Saharudin, K. A., Lai, C. W. and Mat, I. (2009). Studies of Formation of TiO<sub>2</sub> Nanotube Arrays with Various Anodization Parameter and Photocatalytic Application. *Nanomaterials Synthesis & Characterization Conference (nMSC 2009)*, 3<sup>rd</sup>-4<sup>th</sup> Nov 2009, Palace of The Golden Horses, Selangor, Malaysia.
11. Sreekantan, S., **Hazan, R.**, Saharudin, K. A. and Lai, C. W. (2009). TiO<sub>2</sub> nanotube arrays: An ultimate solution for green environment. *Proceeding of the 2<sup>nd</sup> AUN/Seed-Net Regional Conference on Materials Engineering: Material For Changing World*, 19-20<sup>th</sup> November 2009, The Tide Resort, Chonburi, Thailand.
12. **Hazan, R.**, Sreekantan, S. and Mat, I. (2009). Fabrication of highly aligned TiO<sub>2</sub> nanotubes arrays by altering the electrolyte pH value, *International Conference on Nanotechnology (ICONT2009)*, 14-17<sup>th</sup> December 2009, Bayview Hotel, Langkawi Island, Malaysia.
13. Sreekantan, S., **Hazan, R.**, Mat, I., Abdul Khalil, A., Nordin, I. M. S. and Zulkefli, S. S. (2009). TiO<sub>2</sub> nanotubes arrays on Ti – an excellent implant materials, *International Conference on Nanotechnology (ICONT2009)*, 14-17<sup>th</sup> December 2009, Bayview Hotel, Langkawi Island, Malaysia.

14. **Hazan, R.**, Sreekantan, S., Abdul Khalil, A., Nordin, I. M. S. and Mat, I., (2009). Titanium dioxide nanotube arrays for implant, *Solid State Science & Technology (RCSSST2009)*, 21<sup>st</sup>-23<sup>rd</sup> December 2009, Bayview Beach Resort, Penang, Malaysia.
15. **Hazan, R.**, Sreekantan, S., Zulkefli, S. S. and Mat, I. (2011). Effect of biomarker expression of PA6 cells grown on synthesized TiO<sub>2</sub> nanotube arrays, *Translational Science Seminar*, 12-13<sup>th</sup> December 2011, Park Royal Hotel, Penang, Malaysia.
16. Mydin, R. B. S. M. N., **Hazan, R.**, Qazeem, E. Q., Sreekantan, S. and Mat, I., (2011). Telomere length assessment of cells grown on TNA as the marker for genotoxicity profile, *Translational Science Seminar*, 12-13<sup>th</sup> December 2011, Park Royal Hotel, Penang, Malaysia.

#### **Awards:**

1. Sreekantan, S., Ahmad, Z. A., Lockman, Z., **Hazan, R.**, Saharudin, K. A. (2009). TNT – Novel Photocatalyser. International Invention, 1<sup>st</sup>-3<sup>rd</sup> April 2009, Geneva, Switzerland. **Gold Medal with the congratulations of the jury.**
2. Sreekantan, S., Ahmad, Z. A., **Hazan, R.** and Saharudin, K. A. (2009). TiO<sub>2</sub> Nanotubes Arrays an Excellent Smoke Purifier. 20<sup>th</sup> International Invention, Innovation & Technology Exhibition ITEX 2009, 15-17<sup>th</sup> May 2009, Kuala Lumpur, Malaysia. **ITEX Silver Medal.**
3. Sreekantan, S., Ahmad, Z. A., **Hazan, R.**, Saharudin, K. A. and Ibrahim, S. A. (2010). Titano - An Excellent Air Purifier, Malaysia Technology Expo 2010, Kuala Lumpur, Malaysia, 4-6<sup>th</sup> February 2010 - **Gold Medal and Special Awards.**
4. Micrograph Competition – “μ-Size of Banana Leaf” – consolidation prize.
5. Sanggar Sanjung Award (Research Product Category) for the year 2009.
6. Sanggar Sanjung Award (Journal Publication Category) for the year 2009.

# KEJURUTERAAN PERMUKAAN LOGAM TITANIUM UNTUK TINDAKBALAS SEL

## ABSTRAK

Penyelidikan ini fokus kepada pengubahsuaian permukaan titanium dengan morfologi topografi tiub-nano TiO<sub>2</sub>. Tindak balas tiub-nano TiO<sub>2</sub> dan sel stromal tulang PA6 dikaji bagi memahami pengaruh struktur tiub-nano terhadap pertumbuhan sel. Bagi menjayakan objektif penyelidikan ini, kerajang titanium telah diubahsuai kepada tiub-nano TiO<sub>2</sub> yang mempunyai pelbagai dimensi melalui kaedah penganodan dan dicirikan. Tiub-nano TiO<sub>2</sub> bersaiz 25 - 110 nm berjaya dihasilkan di antara 10 V dan 40 V. Rintangan kakisan adalah tinggi bagi sampel yang dianodkan pada 10 V (25 nm-diameter). Panjang tiub-nano TiO<sub>2</sub> adalah 2.2 µm apabila dianodkan selama 3 jam. Fasa anatas, anatas-rutil dan rutil dihasilkan apabila tiub-nano TiO<sub>2</sub> disepuhlindap pada 300 °C, 600 °C dan 700 °C. Struktur tiub juga didapati musnah apabila disepuhlindap pada 700 °C. Fasa anatas mempunyai rintangan kakisan yang tinggi kerana lapisan oksida yang telah dihablurkan menghalang aktiviti kakisan (kadar kakisan = 0.31 nm/tahun). Morfologi sel, perlekatan, kebolehhidupan, imunokimia, aktiviti fosfatase alkali, pemendapan kalsium, *Western Blot* dan *immunophenotyping* dijalankan untuk menilai kesan biologi bagi sel PA6 apabila dikultur di atas tiub-nano TiO<sub>2</sub>. Dari kajian ini, tiub-nano dengan 45 nm-diameter, 2.2 µm-panjang dan mengandungi campuran fasa anatas-rutil meningkatkan pertumbuhan sel PA6. Tiada bahan yang dibebaskan semasa tempoh pengeraman sel PA6 diperhatikan. Kepekatan protein di atas

permukaan tiub-nano lebih tinggi berbanding bahan kawalan kerana luas permukaan dan tapak perlekatan untuk sel memegang substrat adalah lebih besar. Ekspresi *immunostaining* untuk *cytokeratin*, *Bromodeoxyuridine*, CD34, IBMR3 dan propidium iodida adalah positif bagi kesemua sampel. Bagi analisa *immunophenotyping*, sel PA6 adalah positif untuk CD49e, CD51 and CD73. Ini mencadangkan sel PA6 di atas tiub-nano TiO<sub>2</sub> terlibat dalam perlekatan matrik sel luaran, interaksi sel stromal tulang, sistem imun dan pembahagian sel asas *mesenchymal*. Yang pentingnya, sinaran *fluorescence* menunjukkan sel PA6 yang dikultur di atas tiub-nano TiO<sub>2</sub> tidak mengalami perubahan yang mendadak berbanding bahan kawalan. Selepas 14 hari, hydroxyapatite didapati menyelaputi keseluruhan permukaan tiub-nano dan struktur ini meningkatkan pertumbuhan sel PA6. Penemuan ini menjelaskan bahawa tiub-nano merupakan faktor yang penting untuk mengoptimalkan interaksi sel PA6.

# **SURFACE ENGINEERING OF TITANIUM BASED METAL FOR CELL INTERACTION**

## **ABSTRACT**

This research focused on the titanium surface modification with nanotopography morphology of TiO<sub>2</sub> nanotubes. Cell-metal interaction between TiO<sub>2</sub> nanotubes and PA6 bone marrow stromal cells were studied to understand the TiO<sub>2</sub> nanotubes parameters that affect the cell growth. To achieve objective of this research work, titanium foil was transformed into different dimensionalities of TiO<sub>2</sub> nanotubes via simple anodization method and characterized. TiO<sub>2</sub> nanotubes with inner diameter of 25 nm to 110 nm were successfully developed within 10 V to 40 V. Corrosion resistance was higher for sample anodizes at 10 V (25 nm-diameters). The length of the TiO<sub>2</sub> nanotubes arrays were 2.2 μm after 3 hours anodization. Anatase, anatase-rutile and rutile phase was observed when TiO<sub>2</sub> nanotubes subjected to anneal at 300 °C, 600 °C and 700 °C. Tubular structure destroy when anneal at 700 °C. Anatase phase give higher corrosion resistance because crystallized barrier oxide layer hinder the corrosion activity (corrosion rate = 0.31 nm/year). Cell morphology, adhesion, viability, immunocytochemistry, alkaline phosphatase activity, calcium deposition, Western Blot and immunophenotyping were done to evaluate PA6 cells interaction on TiO<sub>2</sub> nanotubes accordingly. From this study, 45 nm-diameter, 2.2 μm-length nanotube and anatase-rutile mixture phase enhanced the PA6 cells growth. No materials elution after 3 days incubation with PA6 cells observed. The protein concentrations on TiO<sub>2</sub> nanotubes were significantly higher than control due to large

surface area and binding sites for cells to anchor to the substrate. Immunostaining expression for *cytokeratin*, *Bromodeoxyuridine*, CD34, IBMR3 and PI was positive on entire samples. From immunophenotyping analysis, PA6 cells were positive for CD49e, CD51 and CD73, suggesting that PA6 cells on TiO<sub>2</sub> nanotube arrays are positively involved in extracellular matrix adhesion, bone marrow stromal cell interaction, immune system and mesenchymal stem cell differentiation. Importantly, fluorescence images show PA6 cells cultured on TiO<sub>2</sub> nanotubes did not have much alteration as compared to control with regard to no significant difference in fluorescence intensity. After 14 days, hydroxyapatite fully covered the TiO<sub>2</sub> nanotube surface and enhanced the PA6 cell growth and viability. These findings indicate that fine-tuning TiO<sub>2</sub> nanotubes will be an essential parameter in optimizing PA6 cell interaction.

# CHAPTER 1

## INTRODUCTION

### 1.1 Introduction

Over the past 20 years, titanium (Ti) and its alloys have been used as implant materials (Park *et al.*, 2010). Biocompatible nature (Vega *et al.*, 2008), excellent mechanical properties and chemical stability (Lee *et al.*, 2009) of Ti makes it a perfect candidate to be used in implant applications. However, implant materials for clinical applications tend to fail because of their poor surface characteristics that enable them to support new bone growth and this will lead to insufficient bonding to juxtaposed bone (Ma *et al.*, 2008), thus slow osteoconductivity (Thian *et al.*, 2006) and healing process. In this case, juxtaposed bone refers to natural bone bonding to implant material. Therefore, lately considerable attention has been focused on Ti surface modification (Chang *et al.*, 2009) such as plasma coating (Hauser *et al.*, 2009 and Wei *et al.*, 2008), etching (Das *et al.*, 2007) and anodization (Yu *et al.*, 2009) to improve surface characteristics for implant material.

Recently, Ti surface was modified to form a self-ordered layer of vertically oriented titanium dioxide (TiO<sub>2</sub>) nanotubes with diameters ranging from 25 and 100 nm by anodization process (Lan *et al.*, 2014). The results revealed that proliferation and cytocompatibility of cells on vertically aligned TiO<sub>2</sub> nanotube surfaces are nanotubes diameter dependent. A nanotube with a diameter of 25 nm seems to have high biocompatibility of epithelial cells in comparison to 50 and 100 nm. Such results indicate that the surface nanostructure of an implant is an important factor for surface cell adhesion and growth. In line with this result, Zhao and co-workers



(2013) observed 30 nm-diameter TiO<sub>2</sub> nanotubes promotes the spread of mesenchymal stem cells (MSC) into polygonal osteoblastic shape. The TiO<sub>2</sub> nanotubes samples promote osteogenesis in absence of an extra osteogenic agent. A 30 nm-diameter TiO<sub>2</sub> nanotubes also generates big nodular alkaline phosphatase (ALP) product and induce extracellular matrix (ECM) mineralization. However, two years ago, Zhao *et al.*, (Zhao *et al.*, 2012) reported 80 nm-diameters of TiO<sub>2</sub> nanotubes give best ability to simultaneously promote MSC proliferation and osteogenic differentiation simultaneously. In 2011, Choe has demonstrated that 50 nm-inner diameter of TiO<sub>2</sub> nanotubes provided good osseointegration such as cell proliferation, migration and differentiation (Choe *et al.*, 2011). Yang *et al.*, suggested that surface treatment with nanotubular TiO<sub>2</sub> surface enhanced the early osteoblast response, such as cell spreading and cytokine release, which is an important factor for subsequent cell functions and bone healing *in vivo* (Yang *et al.*, 2008a). Previous studies by Brammer *et al.*, demonstrate that nanotopography provided nanoscale cue that facilitate cellular probing, cell sensing if more actin cytoskeletal filaments formed lamellipodia and locomotive morphologies (Brammer *et al.*, 2011b). Park's group also showed that adhesion, spreading, growth and differentiation of MSC are critically dependent on the tube inner diameter (Park *et al.*, 2007). Spacing between 15 – 30 nm provided an effective length scale for accelerated integrin clustering/focal contact formation and strongly enhanced cellular activities compared to smooth TiO<sub>2</sub> surfaces. Cell adhesion and spreading were severely impaired on nanotube layers with tube diameter larger than 50 nm resulting reduced cellular activity and experienced programmed cell death. So, Park's group suggested TiO<sub>2</sub> nanotubes with 30 – 50 nm inner diameter represents critical borderline for cell to survive (Park *et al.*, 2007). The cell function altered if

the inner diameter of TiO<sub>2</sub> nanotubes were less than 30 nm and more than 50 nm. The above-mentioned findings are valid generally for the cell response to different topographical nanorough surface and have an important impact on the design and composition of implant surfaces (Gongadze *et al.*, 2011).

## 1.2 Problem statement

Recently, surface topography such as TiO<sub>2</sub> nanotubes have been shown to alter cell behaviors such as adhesion, orientation, differentiation and migration significantly (Koo *et al.*, 2013). It is due to nanotubes topography that can provide more abundant topographical cues similar to dimensional scale of bone collagen fibrils and elasticity resembling bones (Wang *et al.*, 2013). However, the dimensionality (diameter and length) of TiO<sub>2</sub> nanotubes on cell interaction is not well understood. In addition, there have been some inconsistencies in the literature regarding the optimal size of TiO<sub>2</sub> nanotubes for eliciting maximal adhesion, proliferation and cell functionality (Moon *et al.*, 2011; Rajyalakshmi *et al.*, 2011; Lan *et al.*, 2013 and 2014). Therefore, in this research work the effect of diameter and length of TiO<sub>2</sub> nanotubes on cell interaction were systematically studied.

Another factor attribute to the drawback of Ti as implant materials is TiO<sub>2</sub> phases. Among three different crystalline phases of TiO<sub>2</sub>, anatase phase is more favorable for cell adhesion and proliferation due to lower surface contact angle (hydrophilic) and wettability (Koo *et al.*, 2013). In contrast, high surface contact angle (the water contact angle is larger than 90 °) lead to hydrophobic surface, which mimic biological surface such as lotus leaf (Rosario *et al.*, 2004). However, An and group reported that mixture anatase-rutile phase was more favorable for cell

interaction (An *et al.*, 2011). Such contradicting outcomes among research groups cause difficulty for researchers to select the best phase for implant materials. Thus, in order to understand effect of crystal structure on cell interaction, considerable efforts have been devoted to produce stable TiO<sub>2</sub> nanotubes phase that suits cells interaction requirement.

Besides, the selection of cells has also drawn an essential role in determining the cell-metal interaction. Many cells cannot adapt and poorly survive *in vitro* or implanted in the foreign body. This is because foreign material cannot interact properly with cells as they are lack of ECM (Llopis-Hernández *et al.*, 2011). Some efforts have been devoted in the literature to correlate the surface properties to protein adsorption and cell adhesion (Wang *et al.*, 2012). There is still lack of understanding of the cell-metal interaction from an integrated point of view that includes cell adhesion, cell viability and biocompatibility, adsorbed proteins on the nanomaterials surface such as TiO<sub>2</sub> nanotube arrays regarding their dimensionality. The different cells been used in the literature (Huo *et al.*, 2013; Neupane *et al.*, 2011; Roy *et al.*, 2007) also make the analysis on the cell-metal interaction became more complicated. Therefore, detail study on cell-metal interaction specifically on TiO<sub>2</sub> nanotube arrays need to be done by using single cell type (PA6 cells) will be primary concern of this study. PA6 bone marrow cells are well known for a good and main available source of MSC at the present time (Yang *et al.*, 2004 and Ayatollahi *et al.*, 2012a). It is also well ascribed that MSC are best candidates for tissue engineering and cellular therapy of orthopedic musculoskeletal tissues.

Ti has been introduced for biomaterials applications because it owns some of the good biocompatibility and high corrosion resistance. Yu *et al.* (2011) observed that 30 nm-diameter TiO<sub>2</sub> nanotubes had higher resistance of the barrier layer and

lower passive current density ( $I_{\text{pass}}$ ) compared to the smooth Ti. A previous study by Saji and co-workers indicated that the TiO<sub>2</sub> nanotubes surface exhibited passivation behavior and corrosion current density was considerably high. However, the relation within electrochemical corrosion behavior of TiO<sub>2</sub> nanotubes with cell-metal interaction was not reported. Indeed, comprehensive corrosion behavior study and cell-metal analysis would be able to determine the best biomaterials implant.

Other laboratory concerns are materials elution from substrate to cell culture containing serum. This precipitation ions generated mineral nanoparticles with morphologically and chemically identical called nanobacteria (NB). NB is putative living entities are unusual for their small sizes (50-500 nm) have been implicated in numerous diseases involving extraskeletal calcification (Young *et al.*, 2009). Therefore, in the present study, materials elution from TiO<sub>2</sub> nanotubes were analyzed after culturing with PA6 cells. This is to ensure that TiO<sub>2</sub> nanotubes are safe to use as implant materials.

The up-to-date biomarker to characterize cell behaviors has been studied elsewhere (Oh *et al.*, 2013; Huo *et al.*, 2013; Peng *et al.*, 2009). However, no formal consensus has yet been reached on which markers may be best suited for PA6 bone marrow cells. To resolve the PA6 cells behavior during incubation with TiO<sub>2</sub> nanotubes, several biomarkers were tested and discussed.

The hydroxyapatite (HA) coatings formed upon immersion in Simulated Body Fluid (SBF) solution is believed to have similarities to bone apatite (Weng *et al.*, 1997). However, the relation of HA coating surface corrosion behavior and cell interaction study was not discussed by Weng *et al.* (1997). In the present study,

compositional and structural analyses are employed to reveal with the intention of gaining insight into the material response to cell.

In summary, many efforts have been made by researchers (Koo *et al.*, 2013; Llopis-Hernández *et al.*, 2011; Wang *et al.*, 2013; Weng *et al.*, 1997; Yu *et al.*, 2011) to improve biocompatibility of titanium as an implant material by developing TiO<sub>2</sub> nanotubes. However, the effect of nanotubes dimension, crystal structures and HA coating on biocompatibility of PA6 cells are less reported. Therefore, in the present research those parameters were studied.

### **1.3 Objectives**

The objectives of this research are as follows:

- i. To prepare TiO<sub>2</sub> nanotubes with different diameters by an anodization method by controlling potential, time and electrolyte pH.
- ii. To prepare TiO<sub>2</sub> nanotubes with different crystal structures by annealing at different temperatures.
- iii. To investigate TiO<sub>2</sub> nanotubes dimensionality and crystal structure to cell proliferation, viability, attachment, protein adsorption and mineralization.
- iv. To prepare apatite coated TiO<sub>2</sub> nanotubes surface and investigate cell-metal interaction on developed TiO<sub>2</sub> nanotubes surface.

## **1.4 Research outcomes**

The ultimate outcomes of this research project are detailed as follow:

- a) Optimum anodization parameter to form TiO<sub>2</sub> nanotubes for cell-metal interaction is the main outcomes of this research work.
- b) Data on annealing temperature to obtain specific crystal structure of TiO<sub>2</sub> nanotubes.
- c) Optimum dimension and crystal structure for cell proliferation, viability, attachment, protein adsorption and mineralization.
- d) Optimum duration of SBF immersion on apatite formation on TiO<sub>2</sub> nanotubes and its enhancement on cell-metal interaction.
- e) Subsequently, by acquiring this knowledge on the formation of TiO<sub>2</sub> nanotube arrays and study on cell-metal interaction by altering the dimensionality and crystal structure, this research would reveal the viability of using TiO<sub>2</sub> nanotubes as a biocompatible implant material.

## **1.5 Structure of the Thesis**

This dissertation is organized in five chapters consecutively. Chapter 1 is the introduction of the research project, problem statement, objectives and possible outcomes of this research. Chapter 2 introduces the important background of this research work, properties of titanium as implant materials, surface modification of titanium and cell-metal interaction between TiO<sub>2</sub> nanotubes with cells. This includes a comprehensive review on the improvement TiO<sub>2</sub> nanotubes dimensionality and

crystal structure by controlled anodization parameter. Reviews on cellular response to TiO<sub>2</sub> nanotube arrays are also presented. In chapter 3, detailed method of experimental work involved in the preparation and characterization of TiO<sub>2</sub> nanotubes are explained. Also, method to study cell interaction is presented in this chapter. This covers a brief explanation on the characterization equipment, operational principle and sample preparation.

Chapter 4 includes the discussion based on the results obtained from the experiment of TiO<sub>2</sub> nanotube arrays formation and cell-metal interaction study. The content consists of four main parts: (1) the detail investigation on the growth behavior of TiO<sub>2</sub> nanotubes by altering anodization parameter (e.g., applied potential, anodization period and electrolyte pH) and effect of structural characteristics on the surface properties; (2) the crystallization of TiO<sub>2</sub> nanotube arrays at different annealing temperature; (3) cell-metal interaction (cell proliferation, viability, attachment, protein adsorption, mineralization, biomarker (immunostaining and Western Blot) and immunophenotyping) with regard to the TiO<sub>2</sub> nanotubes dimensionality and crystal structure; and (4) HA coating on TiO<sub>2</sub> nanotubes by immersion in SBF and its interaction with PA6 cells. The potential of newly develop TiO<sub>2</sub> nanotube surfaces as implant materials are discussed in detail. Finally, Chapter 5 presents the conclusion of this research work and suggestions for improvement for future study.

## CHAPTER 2

### LITERATURE REVIEW

#### 2.1 Introduction

According to a recent report by World Health Organization (WHO), skeletal injuries that typically involves having patient lie in bed for up to 3 months, prevent most patient from working and thus places large burden on the patient's family (Matityahu *et al.*, 2014). Ideally, effective biomaterials implant is required to overcome aforementioned drawback to stimulate rapid wound healing (Brammer *et al.*, 2008).

Ti and its alloy have been well known implantable materials (Oh *et al.*, 2006). A number of reports have shown that the surface structure of titanium is critical for determining the success or failure of clinical titanium implantations for the purpose of bone, joint, or tooth replacements (Webster and Ejiolor, 2004; Raimondo *et al.*, 2010; Jacobi-Gresser *et al.*, 2013). In the past, numerous studies on implant surface modifications have been performed at the micrometer scale to optimize the surface geometry and profile to best fit cell interactions for adequate bone growth (Kawahara *et al.*, 2004; Li *et al.*, 2005; Pisarek *et al.*, 2011). Recently efforts have been made to improve cell stimulating, biomimetic activities by designing new surface geometries at nanoscale (Lim *et al.*, 2008 and Chiang *et al.*, 2009). Therefore, for the past decade, Kubota have suggested that TiO<sub>2</sub> nanotube arrays grow on Ti metal would be the best candidate as an implant material. The excellent biocompatibility appears to depend on the presence of a passive oxide layer (TiO<sub>2</sub> layer) formed on the surface (Sasaki *et al.*, 2006). In an effort to enhance the



cell implant material interaction and increase lifetime, bioactive ceramic based coatings have been applied to Ti implants (Crawford *et al.*, 2007).

In this chapter, the properties of Ti as implant material is first introduced and reviewed. Then, technique for surface modification of Ti as implant device is discussed. A section on the interaction of TiO<sub>2</sub> nanotubes and cells is also presented.

## **2.2 Ti as biomaterials**

European Society for Biomaterials Consensus Conference defined that biomaterial is a non-viable material used in a medical device intended to interact with biological systems (Carter and Norton, 2007). Recently, demand on the manufacture of synthetic biomaterials arises tremendously in the form of implant and medical devices (Simchi *et al.*, 2011). The aim of biomaterials design is to mimic the biomechanical properties of host tissue (Von Der Mark *et al.*, 2010) and suits its applications. Some of biomaterials and its application are listed in Table 2.1. Among these materials, Ti and its alloys such as Ti-6Al-4V and Ti-6Al-7Nb are widely used in bio-medical applications for instance (e.g. artificial hip, orthopedic or dental implants) because of their high strength-to-weight ratio, good mechanical properties (Table 2.2), biocompatibility (Crawford *et al.*, 2007), high corrosion resistance (low metal ion release) (Macak *et al.*, 2005b and Tsuchiya, 2006), processibility and availability (Freese *et al.*, 2001). Even though Ti commonly used as implant material, they are also utilized as anti-bacteria (Baram *et al.*, 2009), anti-cancer (Kalbacova *et al.*, 2008), drug delivery (Peng *et al.*, 2009) and biosensor (Chen *et al.*, 2010). Figure 2.1 shows the schematic comparison of natural tooth and implant tooth. However, Ti cannot bond directly to living bone after implantation into a host body (Park *et al.*,

**Table 2.1** List of biomaterials and its application.

<b>Implant material</b>	<b>Morphology</b>	<b>Application</b>	<b>Author and Year</b>
<b>Polymer demixing of polystyrenes</b>	Nanometrically high islands	Stents, conduits, and bone repair	De Graaf <i>et al.</i> , (1995) Dalby <i>et al.</i> , (2002) Berry <i>et al.</i> , (2006) Lim <i>et al.</i> , (2012)
<b>Tantalum</b>	Porous	Implant	Bobyn <i>et al.</i> , (1999); Zhang <i>et al.</i> , (1999); Koutsostathis <i>et al.</i> , (2009)
<b>Carbon</b>	Nanotubes	improved tracking of cells, sensing of microenvironments, delivering of transfection agents, and scaffolding for incorporating with the host's body	Harrison and Atala, (2007) Saito <i>et al.</i> , (2009)
<b>Polyaryletherketones (PAEKs)</b>	Porous	orthopedic, and spinal implants	Kurtz and Devine, (2007)
<b>Fe<sub>3</sub>O<sub>4</sub></b>	Nanoparticles	pH-responsive drug release  antibacterial biomaterials for biomedical devices and implants	Gan <i>et al.</i> , (2011) and Chen <i>et al.</i> , (2013) Das <i>et al.</i> , (2013)
<b>HA</b>	Powder compaction	Bone replacement	Saha <i>et al.</i> , (2012)
<b>TiO<sub>2</sub></b>	Foam Thin film Nanotubes	Scaffold Bone implant Nasal surgery (nasal septal perforation repairmen, nasal reconstruction or rhinoplasty and cerebral spinal fluid (CSF) rhinorrhea repairment)	Haugen <i>et al.</i> , (2004) Park <i>et al.</i> , (2011) Lan <i>et al.</i> , (2014)

**Table 2.2** Mechanical properties of selected titanium biomaterials (Freese *et al.*, 2001).

Grade Designation and type	Tensile Strength (MPa)	0.2% Yield Strength (MPa)	Elongation %	Reduction in Area %	Typical Hardness (Rockwell)
Ti CP-1 (Alpha)	241	172	24	30	70 HRB
Ti CP-2 (Alpha)	345	276	20	30	80 HRB
Ti CP-3 (Alpha)	448	379	18	30	90 HRB
Ti CP-4 (Alpha)	552	483	15	25	100 HRB
Ti-6Al-4V (Alpha/Beta)	931	862	15	30	36 HRC
Ti-6Al-7Nb (Alpha/Beta)	862	793	10	25	32 HRC
Ti-15Mo	793	655	22	60	24 HRC
Ti-12Mo-6Zr-2Fe (Beta)	1000	965	15	40	33 HRC
Ti-35Nb-7Zr-5Ta	827	793	20	55	35 HRC

*HRB* = Hardness, Rockwell B Scale, *HRC* = Hardness, Rockwell C Scale.

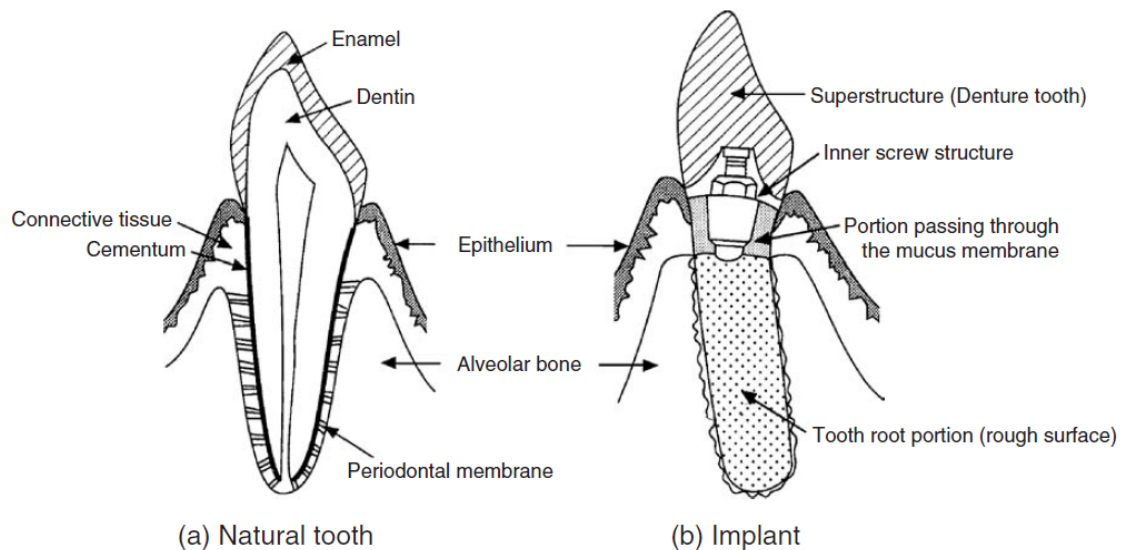


**Figure 2.1** Schematic comparison between natural tooth and implant tooth (Oshida, 2006)

2010). Therefore, the following section provides a method for improving the bone-bonding ability of an implant by modifying Ti surface as investigated in the present study.

### **2.3 Physiological response to implanted materials**

Recently, few studies have reported a correlation between nanoscale surface topography and cell interaction (Conforto *et al.*, 2008; Lamolle *et al.*, 2009; Chamberlain *et al.*, 2011). There are a few biological activities involves before the cell-metal interaction take place. Figure 2.2 shows biological response to material surfaces. Immediately after biomaterial implantation, interaction between water molecules and surface material occur. Then, protein adsorption takes place. Protein that bound to biomaterial surface act as detection sites via specific cell receptors for cell to adhere (integrins) (Jell *et al.*, 2009). Surface chemistry and topography affects the protein quantity, conformation, direction and distribution that bound to biomaterial surface. For instance, direction of adsorbed protein and conformation may hinder cell receptor detection. Cell anchorage to biomaterial surface is crucial for majority of cell type to survive. Focal adhesion sites are combination of proteins that bound to biomaterial surface, receptors at cell membrane and cytoplasmic proteins. Interaction between focal adhesion and cytoskeleton stimulate signal transduction, protein production, gene expression and ECM remodeling. These critical factors subsequently affect cell behavior. These reveal that adaptation of cell adhesion and behavior towards biomaterial surface depends on the type of cell, materials surface and environment.

### **2.4 Biocompatibility of nanomaterials**

Ti is acceptable worldwide for its excellent in implant application due to the biocompatibility properties of Ti. Biocompatibility can be address by an ability of a material to perform with an appropriate host response in a specific application

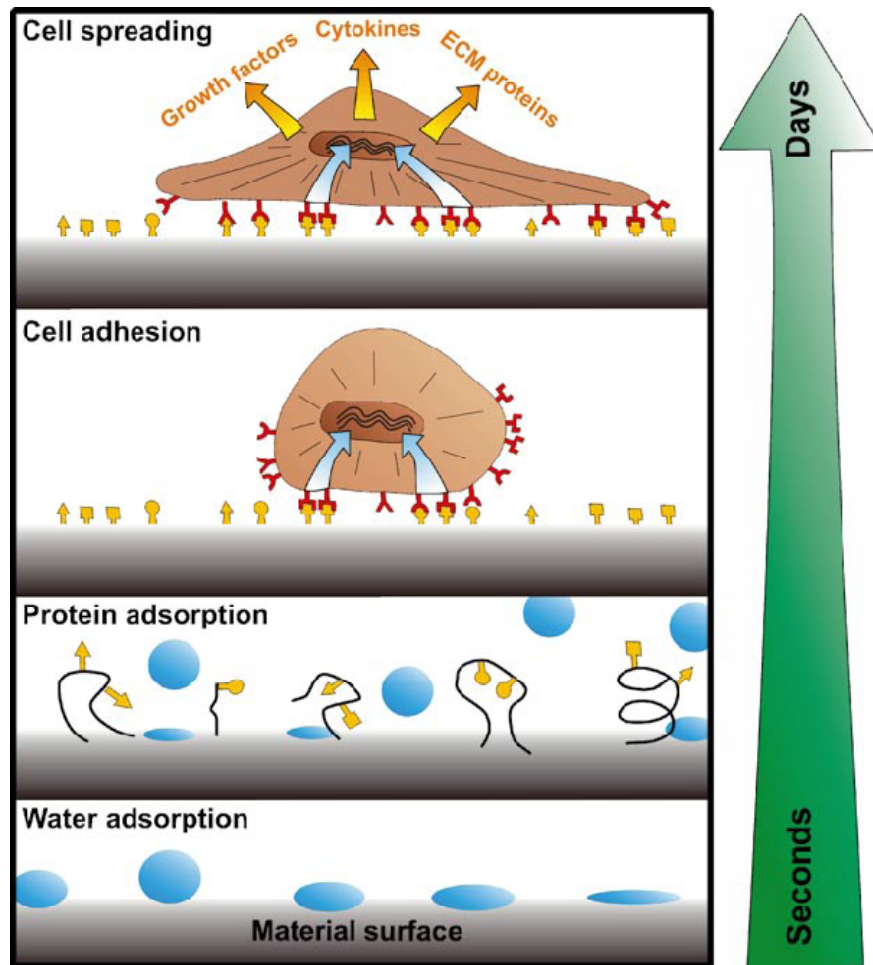


**Figure 2.2** Time line of the biological response to material surfaces (Jell *et al.*, 2009).

(Ratner, 2001). Cytocompatibility and healing process can be improved by modifying Ti surface (Balasundaram *et al.*, 2008).

The high degree of Ti implant biocompatibility is usually ascribed to their ability to form stable and dense oxide layers consisting mainly of TiO<sub>2</sub>. The native oxide layer on Ti is spontaneously grown in most environments whenever has mechanically damaged. These native oxide layers are usually 2-5 nm thick, depending on the redox potential of the surrounding environment. Based on previous

experience with Macak and co-workers (2005a), thicker oxide layers can be grown on the alloys by electrochemical anodization in various solutions.

Nanomaterials formulation exhibited a greater real surface area compared with conventional materials. It is because nanomaterials may significantly influence nanoimplants corrosion behavior (Yu *et al.*, 2009). TiO<sub>2</sub> nanotubes layer has larger surface area compare to conventional materials surface. This matter will affect titanium corrosion resistance (Saji and Choe, 2009). One important characteristic for implant materials is corrosion behavior. TiO<sub>2</sub> nanotubes possessed better corrosion resistance than bare alloys or pure Ti metal (Al-Mobarak and Al-Swayih, 2014). Hollow structure act as perfectly pits because can behave as effective channels for electrolyte to reach implant materials surface. Lower corrosion resistance of these TiO<sub>2</sub> nanotubes resulting from concave shape of tubes bottom and distinctly separated tube bottom with barrier oxide interface (Saji *et al.*, 2009). Thin oxide layer approximately 4 nm on Ti surface make Ti relatively inert and corrosion resistance metal (Ratner, 2001). Pure Ti metal has positive ions that tend to oxidize upon exposure to the environment. Therefore, a systematic research on TiO<sub>2</sub> nanotubes corrosion resistance is a must before clinical trial. Corrosion behavior will be defined either implant materials is biocompatible or not.

#### **2.4.1 Titanium osseointegration**

For the past 30 years, many researches have been developed for improving osseointegration (Ehrenfest *et al.*, 2009). In clinical terms, osseointegration is defined as the stability and stiffness of a joint due to abnormal adhesion and rigidity of the bones which may be the result of injury or disease (Arakeri *et al.*, 2011) of an implant in bone. Fibrous tissue isolates Ti from surrounding bone after implantation

process (Das *et al.*, 2007) by a process known as the foreign body reaction (van den Beucken *et al.*, 2005). Oxidative stress from surgical trauma during and after implantation will create overproduction of free radical and oxygenated derivatives. This phenomenon will thicken TiO<sub>2</sub> layer. Calcium and phosphorus ion from bone matrix are then incorporated within TiO<sub>2</sub> porous layer resulting interface between bone and implant to be highly dynamic (Khor *et al.*, 2006). Unfortunately, contamination and destruction of TiO<sub>2</sub> layer leads to peri-implantitis process. This process is destructive inflammatory process affecting the soft and hard tissues surrounding the implant materials (Ehrenfest *et al.*, 2009). To facilitate osseointegration, an anodization treatment of titanium and its alloys to achieve thicker and more stable TiO<sub>2</sub> based oxides, which are generally favorable for the surface bioactivity (Macak *et al.*, 2005) were studied in the present study.

## **2.5 Cell-metal interaction**

Implantable biomaterials are subjected to several interacting forces whenever they come in contact with the physiological systems (blood, immune system, nervous, digestive, respiratory, reproductive and urinary) and organ in human body. The interaction include the effects of body temperature, body physiological fluids containing several ions and bio-molecules, proteins and cells with various functions (Jackson and Ahmed, 2007). The first interactions are between the cell and surface defines the quality of the cell-metal interaction (Anselme *et al.*, 2010). Integrin receptor acts as an interface between the intracellular and extracellular compartment in cell-metal interaction process. On the extracellular side, integrin interact with ECM and on intracellular side, integrin interact with cytoskeleton and signaling molecules at the adhesion site, called focal adhesion. Figure 2.3 ascribed the

filopodia, lamellipodia and focal adhesion of cell on surface substrate. However, limited information has been discussed in literature on cell–materials interactions. Llopis-Hernández *et al.*, (2011) describe cell-material interaction as a complex bi-directional and dynamic process that mimics biological function to a certain extent the natural interactions of cells with the extracellular matrix. Figure 2.4 shows example ECM covering the substrate surface. Surrounding cells tends to adhere and rearrange adsorbed ECM proteins on the materials surface in a fibril-like pattern. In various literatures, the filopodia act as cell’s tools to explore its surrounding (Le Guehenec *et al.*, 2008; Das *et al.*, 2009; Yu *et al.*, 2010).

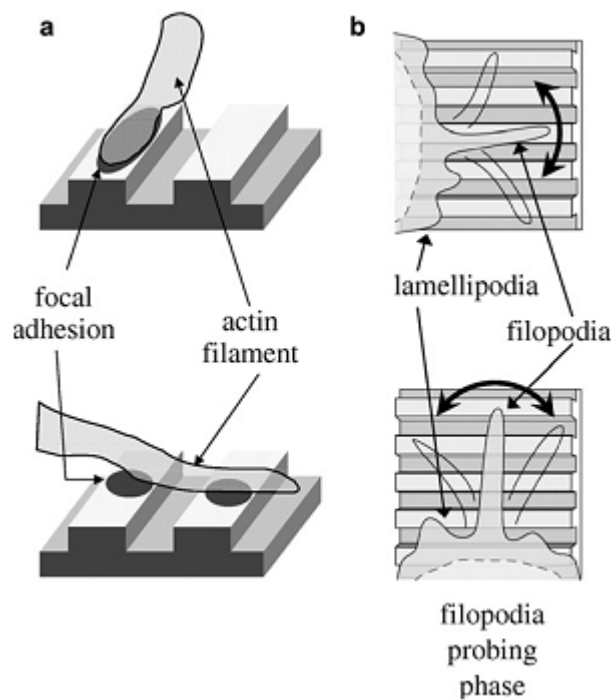


**Figure 2.3** Model for cell alignment on surface substrate. (a) Focal adhesion and actin filament adhere to surface substrate. (b) Filopodia movements are isotropic on surface substrate. Adapted from Anselme *et al.*, (2010).



In general, cell-metal interaction study tends to focus on the initial cell adhesion phase. However, little attention is paid to cell-metal interaction after this stage. First, cells adhered within 24 h, called short-term adhesion. The long-term adhesion represents the strength of cell-metal interface formed within 3 weeks of culture period involving ECM proteins synthesized by the cells themselves and cell-cell interactions can be seen (Anselme *et al.*, 2010). However, cell-metal interaction mechanism which the topographical cue effects the functions of PA6 cells are still not well understood and this has hampered optimization of the biomaterials topography. Therefore, in this work, surface factors such as dimensionality, surface roughness, crystal structure and surface coating were investigated to understand the cell-materials interaction for the next generation orthopedic implants.

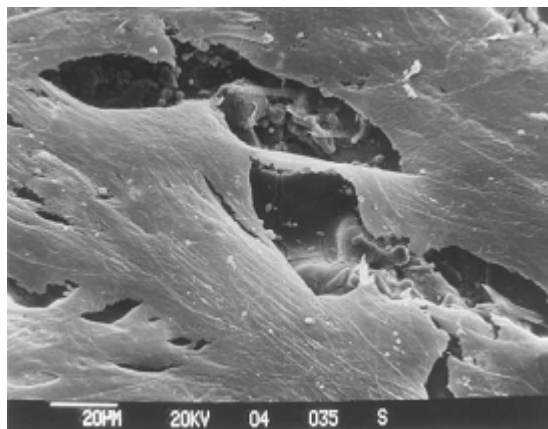


**Figure 2.4** Scanning electron micrograph showing a multilayer of rat bone marrow cells and extracellular matrix covering the substrate surface (Knabe *et al.*, 2002). Bar = 20µm.

### 2.5.1 Cell

An adult human body consists of more than 50 trillion cells and most of these cells are specialized in structure and function (Wynsberghe *et al.*, 1995). Whatever their specific functions, most cells are capable of carrying on life-sustaining

activities such as breaking down food molecules for energy and generating energy-rich adenosine triphosphate (ATP), reproducing, synthesizing chains of polypeptides, engulfing foreign materials and creating new cell structures and getting rid of old ones. Each cells works together with other cells to provide an environment that is compatible with all the process of life (Wynsberghe *et al.*, 1995). Scientists divide cells into four basic parts:

1. The plasma membrane is the outer boundary of the cell. It selectively allows substances to pass into and out of the cell.
2. Cytoplasm is the portion of the cell outside the nucleus and within the plasma membrane. Metabolic reactions take place here with the aid of specialized structures called organelles. The fluid portion of the cytoplasm is called cytosol.
3. The nucleus is the control center of the cell. Within the nucleus are the chromosomes that contain the genes that direct reproduction, information flow and the heredity of cells. The nucleus is a clearly defined body that is separated from the surrounding cytoplasm by a double nuclear envelope.
4. Nucleoplasm is the material within the nucleus.

Table 2.3 shows the selection of cell types to investigate their response and interaction to biomaterials. From Table 2.3, it can be concluded that different cell types gave different cell responses. So, in present days, specific studies are focused to understand the influence of cell type, response and biological mechanisms to specific nanotopography pattern.

**Table 2.3** List of cell type selection to study cell-metal interaction and its information.

<b>Year</b>	<b>Author</b>	<b>Cell type</b>	<b>Information</b>
2014	Lan <i>et al.</i> ,	Human nasal epithelial cells (HNEpC)	Nasal application (nasal septal perforation repairmen, nasal reconstruction or rhinoplasty and CSF rhinorrhea repairmen).
2013	Lan <i>et al.</i> ,	MRC-5 human fibroblasts	Stronger diameter dependence of cell activity
2012	Cao <i>et al.</i> ,	Rat bone marrow stromal cells (BMSC)	Used as dental or orthopedic implants
2011	Brammer <i>et al.</i> ,	MC3T3-E1 mouse osteoblast cells	Aiding in the design of orthopedic implants with improved osseointegrating interfaces.
2011	Chamberlain <i>et al.</i> ,	Bone marrow cells differentiated into macrophage cells	Decreased inflammatory response in medical devices
2011	Choe	MC3T3-E1 mouse osteoblast cells	Used in dental and orthopedic implant materials
2011	Ma <i>et al.</i> ,	Human gingival fibroblasts (HGF)	Use in dental implant abutment
2011	Narayanan <i>et al.</i> ,	MG63 human osteosarcoma cells	Used as orthopedic implant materials
2011	Smith <i>et al.</i> ,	Human dermal fibroblasts and human epidermal keratinocytes	Allow primary integration between the dermis and the transcutaneous implantable devices. Epidermal integration based on subsequent cell signaling and cell-cell attachment.
2011	Yang <i>et al.</i> ,	Osteoblast from fetal rat calvarial cells	Osteoblasts are established cells that respond to the material substrate and have pivotal role at the surface of implant materials with the secretion of many cytokines involves in bone remodeling
2010	Yu <i>et al.</i> ,	MC3T3-E1 mouse osteoblast cells	Used as implantation materials.
2008	Das <i>et al.</i> ,	Osteoblastic precursor cell line (OPCI)	Preferential cell attachment on rough surface compare to smooth surface.

### **2.5.2 PA6 cells**

PA6 or MC3T3-G2 cells are stromal cell line derived from newborn mouse calvaria (Turksen, 2002). Bone marrow stromal cells are a critical cellular element of the bone marrow microenvironment and support the production of blood cells from the bone cavity in adults (Milwid *et al.*, 2013). In certain situation, PA6 cells mono layer can be used as feeder cells that support sustained generation of various hematopoietic progenitor types. PA6 cells support the differentiation of cells resembling osteoclasts in co cultures with spleen cells (Krauser *et al.*, 1994).

### **2.6 Nano-scale surface engineering on Ti**

The term ‘surface engineering’ was used for the first time in England in the 70s. Different aspect of thermal spraying and welding are focusing at the beginning before progressively broadened its range of attention. Then, Wolfson Institute for Surface Engineering was formed at University of Birmingham. That institute mainly concern with problem stemming from surface diffusion treatment with vacuum technology at the beginning. Next, the activity broadening its scope to various technique of surface layers formation. Surface engineering is a science discipline including surface layers manufacturing processes (coating and exterior layer for the purposes of scientific and technology) related phenomenon and performance effects (Burakowski and Wierzchoń, 1999).

Surface modification can be derived by transformation of structure, morphology and material surface composition without leaving the bulk mechanical properties (Hanawa, 2009). The aim of Ti surface modification is to produce fine porous layer on biomaterials. Specifically, cavities and high surface area of

biospecies, precursor's adsorption and anchoring were exploited (Macak *et al.*, 2005b). To further improve Ti bioactivity, biocompatibility, the interface between bone and implant and implant anchorage to bone, different surface modification methods have been explored (Tsuchiya, 2006).

Typically, two different strategies have been developed. In the first approach by incorporating inorganic phases such as calcium phosphate on or into TiO<sub>2</sub> layer interface chemically was improved. This inorganic chemical modification, bone regeneration is stimulated and biochemical interlocking between bone matrix proteins and surface materials increase. Conversely, biochemical surface modification is differ from first strategy and refer to organic molecules incorporation such as protein, enzymes or peptides to persuade specific cell and tissues responses (Ehrenfest *et al.*, 2009).

For second approaches, the interface is improved physically by surface topography architecture. At micrometer stage, rough surface create higher developed area rather than smooth surface. This rough surface increase bone anchorage reinforced the biomechanical interlocking of the implant with bone up till certain level of roughness. At nanometer stage, the roughness increase surface energy to improve protein matrix adsorption, bone cell migration, proliferation and osseointegration (Ehrenfest *et al.*, 2009). To date, anodization of Ti has been investigated because can be easily create biological-inspired nanometer roughness (Balasundaram *et al.*, 2008). From Table 2.4, nano-scale topography of TiO<sub>2</sub> provides adhesion sites for protein help cell proliferation into 3D formation and facilitate in cell differentiation as compared to other surface morphology. Wu *et al.*, (2008) indicate the potential use of spin-coating materials for orthopedic and implant materials. Spin coating significantly improved adhesion strength, chemical stability

**Table 2.4** List of surface engineering approaches to achieve geometrical structuring of TiO<sub>2</sub> surface.

<b>Year</b>	<b>Author</b>	<b>Surface engineering</b>	<b>Morphology</b>	<b>Finding</b>
<b>2001</b>	Casaletto <i>et al.</i> ,	Metal organic chemical vapor deposition	Thin film	Higher amount of organic species found on the substrate surface
<b>2005</b>	Li <i>et al.</i> ,	Polymeric sponge replication	Porous TiO <sub>2</sub> sponge	Nontoxic and favorable for cell attachment
<b>2009</b>	Chiang <i>et al.</i> ,	Anodization	Nano-network layer of TiO <sub>2</sub>	Greater amount of proteins on nano-scale TiO <sub>2</sub> network. Help human bone marrow stem cells (hMSC) proliferate to 3D formation in vivo Facilitate hMSC to differentiate toward osteogenic lineage
<b>2010</b>	Raimondo <i>et al.</i> ,	Electron beam evaporation	Micron rough surface features and higher degree of nanometer surface features	Increase surface energy and promote surface osteoblast and endothelial cell adhesion

and able to form apatite layer in SBF compared to HA coat Ti-6Al-4V. Based on the literature review of this section, it is important to optimized implant materials regarding their surface characteristic (e.g. chemistry, topography, surface energy and morphology (Bauer *et al.*, 2008) before implantation.

### 2.6.1 TiO<sub>2</sub> nanotube arrays

An approach for synthesis of highly ordered and vertically oriented TiO<sub>2</sub> nanotubes on Ti and Ti-alloy substrates have been discovered in 1999. Basically, anodization of the substrates was performed in a fluoride containing electrolyte under specific electrochemical conditions that lead to self-organize TiO<sub>2</sub> nanotubes. Up to now, several generations of nanotubes have been brought forward (Kalbacova *et al.*, 2008) to further improve its dimensionality.

For pure Ti, the compact TiO<sub>2</sub> layer thickness increase gradually with the growth rate of 2.5 nm/V up to applied voltage where dielectric breakdown of the oxide occurs at 100 - 200 V. Ti anodization in electrolytes contain F<sup>-</sup> ion at 10 - 20 V produced porous structures ( $\pi$ -TiO<sub>2</sub>) consist of nanotubes with 100 nm range diameter (Macak *et al.*, 2005b) and a length of ~ 500 nm (Tsuchiya, 2006). Figure 2.5 shows TiO<sub>2</sub> nanotubes morphology and cross sectional view. Throughout anodization process, the Ti foil surface color generally transforms from purple to blue, yellow, red, and then lastly light red (Quan *et al.*, 2005). Through this technique, TiO<sub>2</sub> nanotubes with a diameter ~ 100 nm could be developed.

The construction of the nanotube structures on titanium during anodization is because of the competition between TiO<sub>2</sub> growth and TiO<sub>2</sub> dissolution. Throughout the Ti foil anodization nanotube structures are produced through two processes: field-enhanced Ti oxidation and field-enhanced oxide dissolution. There are two